J Nanopart Res (2026) 28:79
https://doi.org/10.1007/s11051-026-06595-0

RESEARCH

Synthesis and characterization of reduced graphene oxide/silica composite for anti-cancer drug delivery system

Tugba Okur · Deniz Gul · Muge Sari Yilmaz

Received: 12 December 2025 / Accepted: 18 February 2026
© The Author(s) 2026

Abstract Cancer poses a serious global health problem, responsible for the deaths of millions of people annually. In this context, the design of drug delivery systems has attracted notable interest due to minimizing the adverse effects of cancer drugs on living cells. This study aims to synthesize an efficient carrier for the anticancer agent imatinib mesylate (IM) through the synthesis of a composite material combining mesoporous silica with reduced graphene oxide (rGO@ms) via green synthesis. The release behavior of IM was systematically assessed under different pH conditions (5.0, 6.0 and 7.4) to simulate diverse environments. IM-loaded and unloaded rGO@ms were characterized using UV–Vis spectroscopy, X-ray diffraction (XRD), Fourier-transform infrared spectroscopy (FTIR), and field emission scanning electron microscopy (FESEM) analysis methods. The drug loading capacity of rGO@ms was calculated as 27.79%. Over a 50-h period, IM-loaded rGO@ms was found to have released approximately 80% at pH 5.0, 58% at pH 6.0 and 19% at neutral pH (7.4). The release was significantly higher at pH 5.0, which is attributed to the easier breakdown of the bond between the drug and carrier in an acidic environment. The synthesized composite, which shows favorable release characteristics at lower pH levels, has great potential for cancer treatment. Moreover, the drug release mechanism of the composite was found to closely follow the Korsmeyer–Peppas kinetic model.

Keywords Reduced graphene oxide · Green synthesis · Mesoporous silica · Composite · Drug delivery

Introduction

Cancer is a severe illness that is commonly seen worldwide and is a leading cause of mortality [1]. Since the main cancer treatment methods currently applied, such as chemotherapy, radiation, and surgery, damage healthy cells, discovering new treatment methods has become a crucial strategy to destroy tumor cells [2]. Drug delivery systems (DDS) are designed to target specific sites and reduce the side effects of chemotherapeutic drugs. The primary purpose of DDS is to achieve controlled release of therapeutic cancer drugs that have been previously loaded onto their surfaces in the presence of external stimuli such as pH, heat, and light that affect the release kinetics [3, 4]. Accordingly, the development of biocompatible and highly effective drug delivery systems compatible with cancer treatments is gaining critical importance in the oncological field [5, 6]. Recent improvements have included various drug

T. Okur · D. Gul · M. Sari Yilmaz (✉)
Department of Chemical Engineering, Yildiz Technical University, 34220 Istanbul, Türkiye
e-mail: mugesari@yildiz.edu.tr

Published online: 09 March 2026

carriers, such as liposomes, dendrimers, micelles, and mesoporous materials [7]. These effective carriers aim to prolong the time of drugs in the body, increase drug tolerance, and minimize adverse outcomes and the toxicity of cancer drugs [8].

Graphene and its hybrids have become remarkable biomaterials in contemporary research, enabling development as a class of biosensors, cell sensors, and carrier vehicles for drug delivery [9]. Graphene oxide (GO) has unique properties such as excellent biocompatibility and the ability to be functionalized with covalent and noncovalent materials to enhance surface activity, making it a suitable option for systems that precisely deliver drugs. In addition to the aforementioned, it retains some oxygenated functional groups, predominantly carboxylic acid at the edges of the hexagonal planes and hydroxyl and epoxy groups on both sides of the layers, allowing the drug to be loaded via van der Waals forces [6, 10]. rGO is a graphene hybrid obtained from GO by a diverse array of reduction routes, such as chemical vapor deposition, chemical/thermal reduction, and micromechanical methods [11]. Chemical reduction of GO involves the use of hazardous reducing agents such as sodium borohydride, dimethylhydrazine, and hydrazine hydrate, resulting in trace amounts of toxic components in the final product, restricting its use in biological applications [12]. Plants and their derivatives are considered one of the most potential green reducing candidates to overcome these limitations [13]. Green reduction offers unique advantages, including the absence of toxic chemicals, non-hazardous nature, and low cost [14, 15]. Bay leaf, one of the green reducing candidates, is a plant native to the Southern Mediterranean region. It encompasses numerous significant functional components, including proteins, organic acids, free sugars, phenolic compounds, and flavonoids, which facilitate the reduction of metallic ions to produce and stabilize nanoparticles [16, 17].

Mesoporous silica (ms) is considered a potential candidate for drug delivery due to its large surface area, biocompatibility, and high pore volume [18, 19]. Recent research suggests that ms can offer high drug delivery efficiency by releasing its payloads in response to certain stimuli, such as the acidic environment of tumors [20]. Despite the unique advantages of ms, its high pore volume can lead to failure of the desired efficacy of the targeted drug, leading to rapid or unintended drug release. This limitation can be significantly mitigated by adding a biocompatible and environmentally friendly layer to the ms surface [21]. Liu et al. developed a multifunctional nanocarrier comprising rGO coated with an ms shell, demonstrating pH-responsive release of doxorubicin (DOX) with increased drug release under acidic conditions [22]. Similarly, Khanmohammadi et al. reported an rGO/SiO_2 nanocomposite for quercetin delivery, showing enhanced drug release at acidic pH levels [23]. Furthermore, Guo and colleagues designed an rGO/MSN/C18PEG composite for photothermal chemotherapy, where DOX was loaded via non-covalent interactions, resulting in improved anticancer efficacy [18]. Mesoporous silica packed with graphene oxide (GO-MSN) nanosheet was developed for the controlled release of rizatriptan benzoate (RiB) and the in vitro RiB release from the nanosheet was found to be 70.74% [24]. pH-sensitive chitosan/graphene oxide (CS/GO)–based microspheres were synthesized and used as drug carriers for amoxicillin, and it was found that the system containing 15% GO exhibited high drug loading (~89%), controlled and pH-responsive release, good biocompatibility, and strong antibacterial activity [25]. The DOX-loaded HN-1–functionalized PEGylated nanoscale GO exhibited clear pH-responsive drug release, reaching ~70% release at pH 5.6, decreasing to ~30% at pH 6.6, and remaining minimal at pH 7.4 due to the weakening of hydrogen bonding and π–π interactions under acidic conditions [26].

Herein, we report a novel rGO@MS nanocarrier synthesized via green reduction using bay leaf extract for the delivery of the anticancer drug IM. This study represents the first use of bay leaf extract, a cost-effective, environmentally friendly, and biocompatible reducing agent, in the synthesis of a rGO@ms-based drug carrier. IM loading efficiency was evaluated, and IM release was studied at three different pH values (5.0, 6.0, and 7.4).

Experimental section

Materials

Sodium nitrate ($NaNO_3$), potassium permanganate ($KMnO_4$), hydrogen peroxide (H_2O_2), and sulfuric acid (H_2SO_4, 95–97%), tetraethyl orthosilicate ($SiC_8H_{20}O_4$, 99%), sodium hydroxide (NaOH, > 97%), ethanol (C_2H_6O, 96%), hexadecyltrimethylammonium bromide ($C_{19}H_{42}BrN$), and ammonia solution (25%) were

purchased from Merck. Graphite powder (99.99% pure) was supplied by ABCR. The active ingredient IM ($C_{30}H_{35}N_7O_4S$) was supplied by Deva Holding. Sodium phosphate dibasic ($Na_2HPO_4, \geq 99.9\%$) and potassium dihydrogen phosphate ($KH_2PO_4, \geq 98\%$) were purchased from AFG Scientific.

Preparation of GO

GO powder was synthesized by a modification of Hummers' method. Initially, a mixture containing powdered graphite, $NaNO_3$, and H_2SO_4 solution (96.7%) was prepared in an ice bath and stirred for a specific period using a magnetic stirrer. While the temperature was maintained below 5 °C, $KMnO_4$ was gradually added throughout the process. The mixture was then removed from the ice bath and stirred for a specific time under 35–40 °C conditions. Deionized water was then added, and the mixture was continuously stirred for 1 h. To prevent the temperature of the solution from exceeding 40 °C, H_2O_2 (35.7%) was introduced and agitated for two more hours. Finally, the resulting solution was thoroughly washed and filtered with distilled water and then dried in an oven at 50 °C overnight.

Preparation of reduction solution

Bay leaves collected from the garden of Yildiz Technical University were cleaned and freed from debris such as lint and dust for the reduction solution. After drying at room temperature, the bay leaves were crushed and sieved to 90 µm. A mixture of sieved bay leaves and distilled water was placed in a flask and shaken at 80 °C for a specified period to extract the leaves. The yellow solution was filtered at the end of this period, and the resulting extract was stored at 4 °C.

Synthesis of rGO@ms

Initially, GO (1.5 mg/mL), CTAB (2 mg/mL), and a 25% NH_3 solution (1.5% v/v) were introduced into a mixed solvent (H_2O/EtOH, = 2:3 (v/v)). The suspension was then subjected to ultrasonication followed by magnetic stirring. Subsequently, TEOS was introduced incrementally while maintaining constant agitation. The resulting mixture was filtered and washed with ethanol and water. The filtrate was combined with ethanol and stirred for a set time at 60 °C. After an additional ethanol wash, it was vacuum dried at a controlled temperature for 12 h. Bay leaf extract was introduced to the mixture and refluxed for 12 h to achieve GO reduction. Upon completion, the mixture was filtered and washed with water and ethanol, and the final solid was vacuum dried at a determined temperature and time. The synthesis process of the rGO@ms is illustrated in Fig. 1.

Characterization

To evaluate the drug release behavior of rGO@ms, a Hanon I8 UV–VIS spectrophotometer was utilized, with the maximum absorbance wavelength for IM identified at 265 nm. The crystallographic phase structure of samples was recorded using a PANalytical X'Pert PRO X-ray diffractometer with CuKα radiation ($\lambda = 0.154$ nm) at an operating voltage of 45 kV and a current of 40 mA. FTIR spectra were conducted for different samples using a Perkin Elmer Spectrum One spectrometer, employing the KBr pellet technique. The surface morphology of rGO@ms was acquired using a Zeiss EVO LS 10.

Drug loading studies

In the drug-loading experiment, rGO@ms (2 mg/mL) and IM (1 mg/mL) were suspended in PBS solution at pH 7.4. The suspension was incubated at 150 rpm for 24 h at room temperature to promote effective interaction and drug adsorption. Then, the IM-loaded rGO@ms was collected by filtration, subsequently washed a few times with distilled water and PBS to remove unbound drug, and vacuum dried at 70 °C for 12 h. The IM drug loading capacity (LC) of the composite was calculated using the following equation:

$$LC(\%) = \frac{Amount\ of\ IM\ in\ composite\ (mg)}{Amount\ of\ composite\ (mg)} \times 100 \quad (1)$$

Drug release studies

Compared to the neutral pH of human plasma (pH = 7.4), the acidic pH of cancer cells is associated with excess metabolites resulting from rapid multiplication. Therefore, PBS at different pH gradients (5.0, 6.0, and 7.4) was prepared to simulate diverse

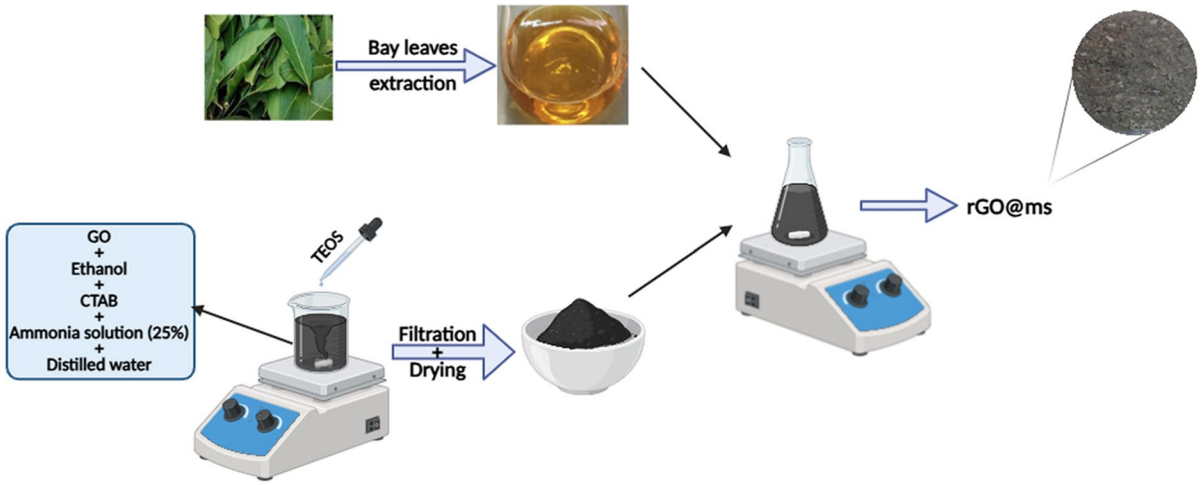


Fig. 1 Schematic of the rGO@ms synthesis

microenvironments, and the pH-responsive IM release behavior of rGO@ms was investigated [27, 28].

The IM release profile of the IM-loaded rGO@ms was achieved using the dialysis bag diffusion method at 37 °C. IM-loaded rGO@ms was placed in a dialysis membrane and immersed in PBS with discrete pH. 4 mL samples were collected at predetermined time intervals, and an equal volume of fresh PBS was added to replenish the release medium. The IM concentration released into PBS was quantified by UV–Vis spectrophotometry, allowing evaluation of IM release kinetics over time.

Drug release kinetic study

The primary objective of kinetic analyses in controlled drug delivery systems is to examine the temporal variations of medication dose forms and their release profiles. These systems utilize mathematical models to determine the mechanisms of drug release. Using appropriate mathematical models, it is possible to determine the drug release rate and mechanism across various drug delivery systems [29]. In this study, the IM release mechanism of rGO@ms was investigated by processing the obtained drug release data and fitting it into different kinetic models, including zero-order, first-order, Higuchi, and Korsmeyer–Peppas. The corresponding mathematical expressions for the kinetic models are presented in Table 1. The correlation coefficient (R^2) achieved from kinetic models reveals the best accordance of the relevant kinetic models with the experimental assays.

Table 1 Kinetic model expressions for drug release

Kinetic model	Equation
Zero order	$w = k_0.t$
First order	$\text{Log}\ (100 - \text{w}) = \text{Log}\ 100 - k_1.t$
Higuchi	$w = k_{\text{H}}.t^{0,5}$
Korsmeyer-Peppas	$\frac{M_t}{M_\infty} = k.t^n$

Here, k_0, k_1, k_H, and k are the drug release rate constants, w is the percentage of drug release at a given time t, n is the diffusion exponent, and $Mt/M\infty$ is the value for released drug in solute [29]

Results and discussion

Characterization of rGO@ms and IM-loaded rGO@ms

The XRD patterns for rGO@ms and GO are displayed in Fig. 2a. In the XRD graph of GO, a peak at $2\theta = 10.83°$ ($d = 0.817$ nm) with the (001) plane and a peak at $2\theta = 42.08°$ ($d = 0.215$ nm) with the (100) plane are observed. The complete disappearance of these characteristic GO peaks with the composite production proves that the GO reduction process with bay leaf was successful. In addition, the broad characteristic peak observed at $2\theta = 22.7°$ indicates the formation of amorphous SiO_2 [30].

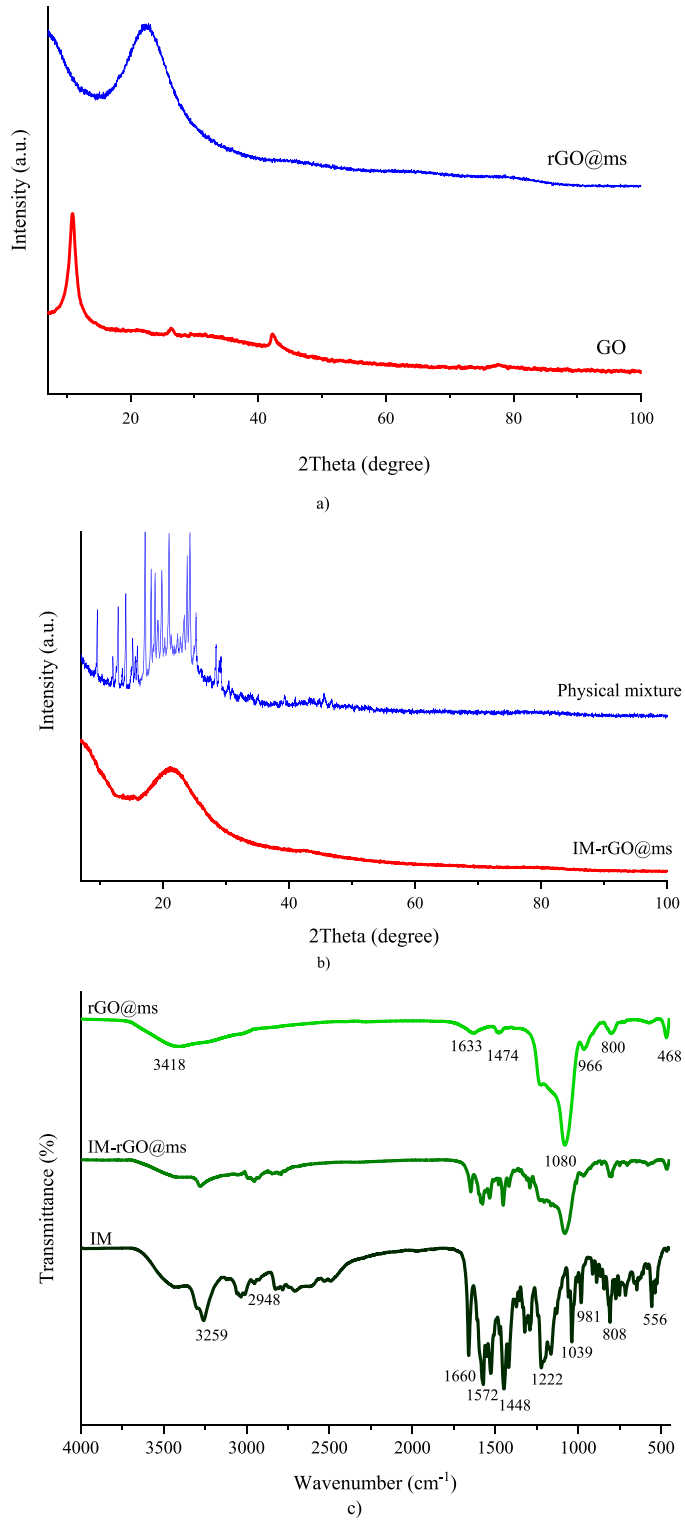


Fig. 2 Structural and chemical characterization of the samples. XRD patterns (**a**, **b**); FTIR spectra (**c**)

The XRD patterns of the IM-loaded rGO@ms and physical drug combination are represented in Fig. 2b. When comparing the two patterns, the physical mixing of the drug and the rGO@ms demonstrates strong crystalline peaks of IM. After IM loading, rGO@ms indicated that the amorphous silica structure remained intact; however, there were extremely faint IM crystal peaks in the 2θ = 12–16° region. It seemed that IM molecules were effectively absorbed by the rGO@ms structure.

The FTIR spectra of rGO@ms, pure IM, and the IM-loaded rGO@ms are shown in Fig. 2c. In the spectrum of rGO@ms, the O–H stretching vibration from the silanol (Si–OH) groups is linked to the peak at 3418 cm^{-1} in the rGO@ms spectrum. The C = O (carbonyl and carboxyl) group is represented by the peak at 1633 cm^{-1}, whereas the aromatic C = C stretching vibration is responsible for the peak at 1474 cm^{-1}. The Si–OH vibrations on the surface of rGO@ms are responsible for the peak at 966 cm^{-1}, whereas the asymmetric stretching, symmetric stretching, and vibrations of Si–O–Si bonds are responsible for the peaks at 1080, 800, and 468 cm^{-1} [31, 32]. In the spectrum of IM, the absorption band observed at 3259 cm^{-1} corresponds to N–H stretching vibrations, while the peaks near 2948 cm^{-1} are attributed to $=CH_2$ stretching. The bands around 1572 cm^{-1} and 1660 cm^{-1} are associated with C = O stretching vibrations. The absorption band at 1448 cm^{-1} corresponds to the stretching vibrations of aromatic C = C and C = *N* bonds. The peak at 1039 cm^{-1} is assigned to C–O stretching vibrations, whereas the band at 808 cm^{-1} arises from the out-of-plane deformation of aromatic C–H groups [33, 34].

Figure 3 presents a comparative analysis of the UV–Vis spectra for rGO@ms, pure IM, and IM-loaded rGO@ms. Notably, the characteristic absorption peak observed at 265 nm in both IM and the IM-loaded rGO@ms is absent in the spectrum of the unloaded rGO@ms. This distinct spectral feature provides strong evidence for the successful incorporation of IM within the rGO@ms matrix.

The surface morphology of rGO@ms was assessed by the FESEM technique. The related FESEM image and the elemental mapping are displayed in Fig. 4. rGO@ms exhibits a layered structure and both large and small spherical particles with diameters of about 200 and 550 nm. The layered structure indicates the

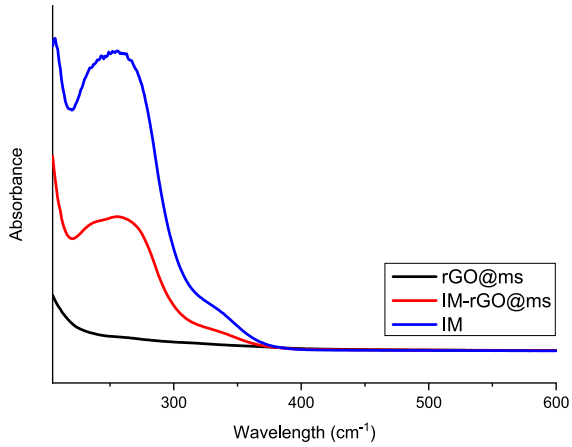


Fig. 3 UV/Vis spectra of rGO@ms, pure IM, and IM-rGO@ms

rGO structures, while the spherical form exhibits the silica structure as anticipated, according to elemental mapping analysis. The FESEM image demonstrates that spherical msilica are coated by the planar rGO layer.

The LC value of rGO@ms was found to be 27.79%, indicating that IM can be effectively loaded into the composite. It can be suggested that IM loading onto the rGO@ms composite involves multiple mechanisms, including electrostatic attraction between IM molecules and the rGO@ms structure, π–π interactions and hydrogen bonding between IM and the composite surface, as well as adsorption of IM within the mesoporous silica pores, consistent with previous reports (Fig. 5) [35–38].

Drug release studies

Figure 6 shows the cumulative drug release profile of the IM-loaded rGO@ms at different pH levels. The amount of IM released over time depended on the pH level, with more IM being released as the pH level dropped. Over the course of 50 h, about 80% of IM was released from IM-loaded rGO@ms at pH 5.0, 58% at pH 6.0, and 19% at pH 7.4. The protonation of oxygen-containing functional groups on the rGO surface and increased protonation of IM result in a higher release rate in acidic environments. This

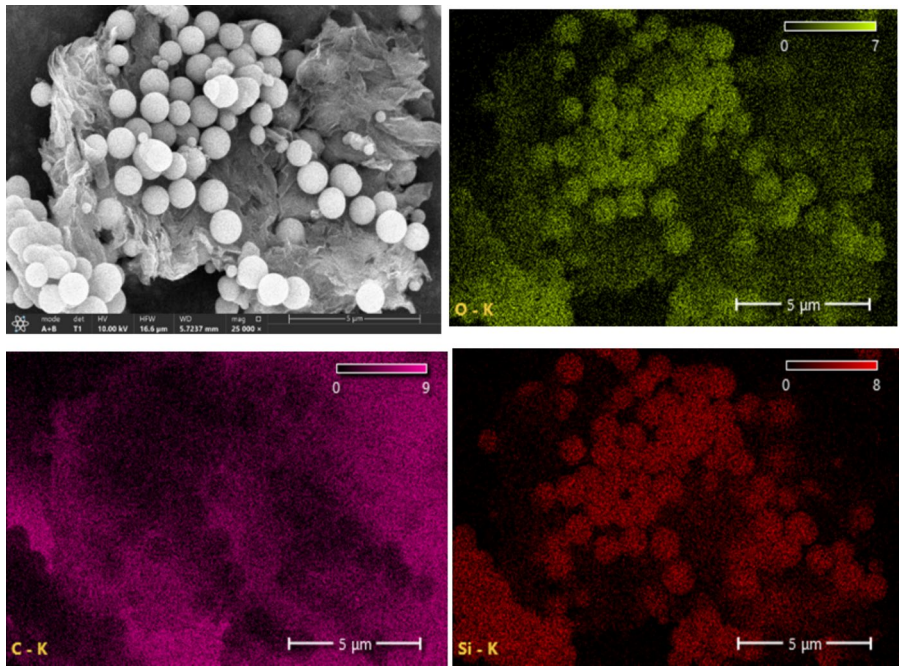


Fig. 4 FESEM image of rGO@ms and corresponding elemental mapping images

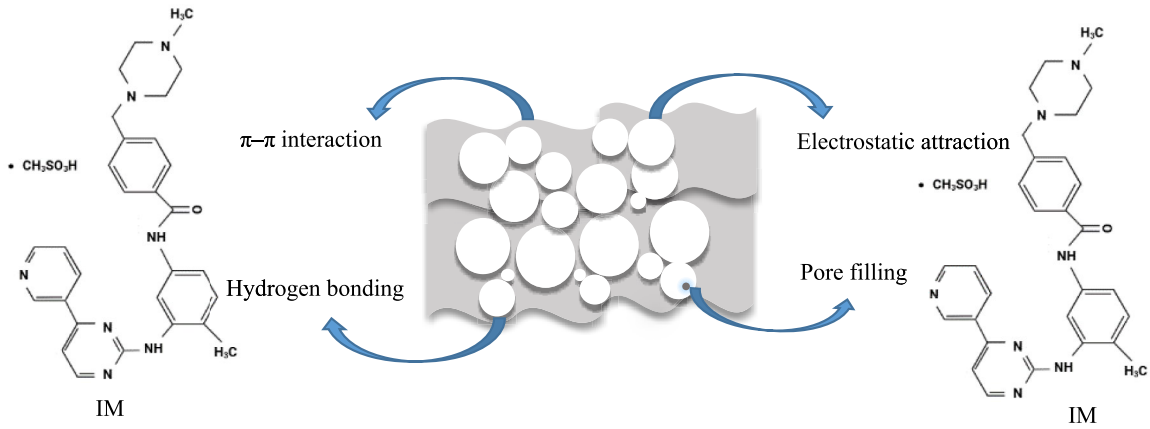


Fig. 5 A probable IM loading mechanism

makes the electrostatic attraction and π–π interactions between the IM and the carrier matrix less strong. However, at physiological pH (7.4), less protonation and stronger interactions between the drug and the matrix make the release happen much more slowly. Since tumor microenvironments are acidic, the pH-sensitive release behavior suggests that rGO@ms is a good choice for delivering drugs to tumors.

Drug release kinetic studies

Figure 7 illustrates the IM release kinetics of the rGO@ms at pH 5.0 according to the zero-order, first-order, Korsmeyer–Peppas, and Higuchi kinetic models. Table 2 presents a summary of the calculated kinetic parameters derived from the various applied kinetic models. Upon examining the coefficients

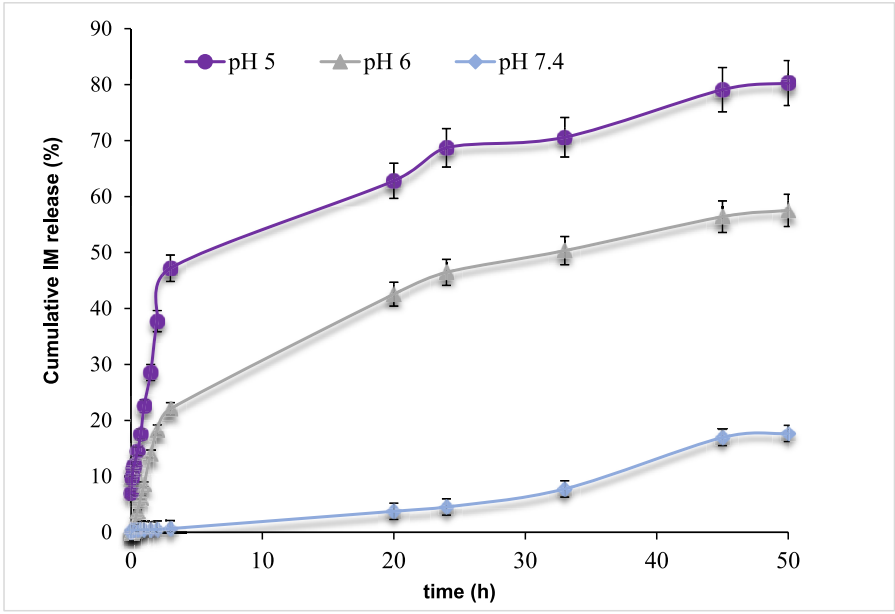


Fig. 6 Drug release studies of IM from rGO@ms at pH of 5.0, 6.0, and 7.4

Table 2 Fitting parameters of the kinetic models

Kinetic model	Parameters	Value
Zero order	k_0	1.44
	R^2	0.8293
First order	k_1	0.01
	R^2	0.9323
Higuchi	k_H	10.67
	R^2	0.9391
Korsmeyer-Peppas	K	1.25×10^{-4}
	n	2.87
	R^2	0.9658

of determination (R^2) presented in the table, it is observed that the optimal fit is achieved with the Korsmeyer–Peppas kinetic model. The diffusion exponent (n) in this model characterizes the specific type of release mechanism. Values of $n \leq 0.45$ denote Fickian diffusion, $0.45 < n < 0.89$ signify an anomalous (or non-Fickian) diffusion, and $n > 0.89$ indicate non-Fickian transport. The n value determined in this study was greater than 0.89, indicating that IM was released from the system via an anomalous diffusion mechanism and that multiple release mechanisms operate simultaneously, indicating a super case II transport behavior [39].

Conclusion

Synthesis of rGO@ms was undertaken as a potential drug carrier for the anticancer drug IM. By eschewing the use of toxic chemicals traditionally utilized in GO reduction, bay leaf extract was used as an eco-friendly reductant in green synthesis. Drug-loading assays revealed a loading efficiency of 27.79%, and analyses validated the inclusion of IM into the rGO@ms matrix. The results accomplished a pronounced pH-responsive release behavior, with cumulative release percentages of approximately 80% at pH 5.0, 58% at pH 6.0, and 19% at pH 7.4 over a period of 50 h. The enhanced release in acidic conditions is attributed to the protonation-induced

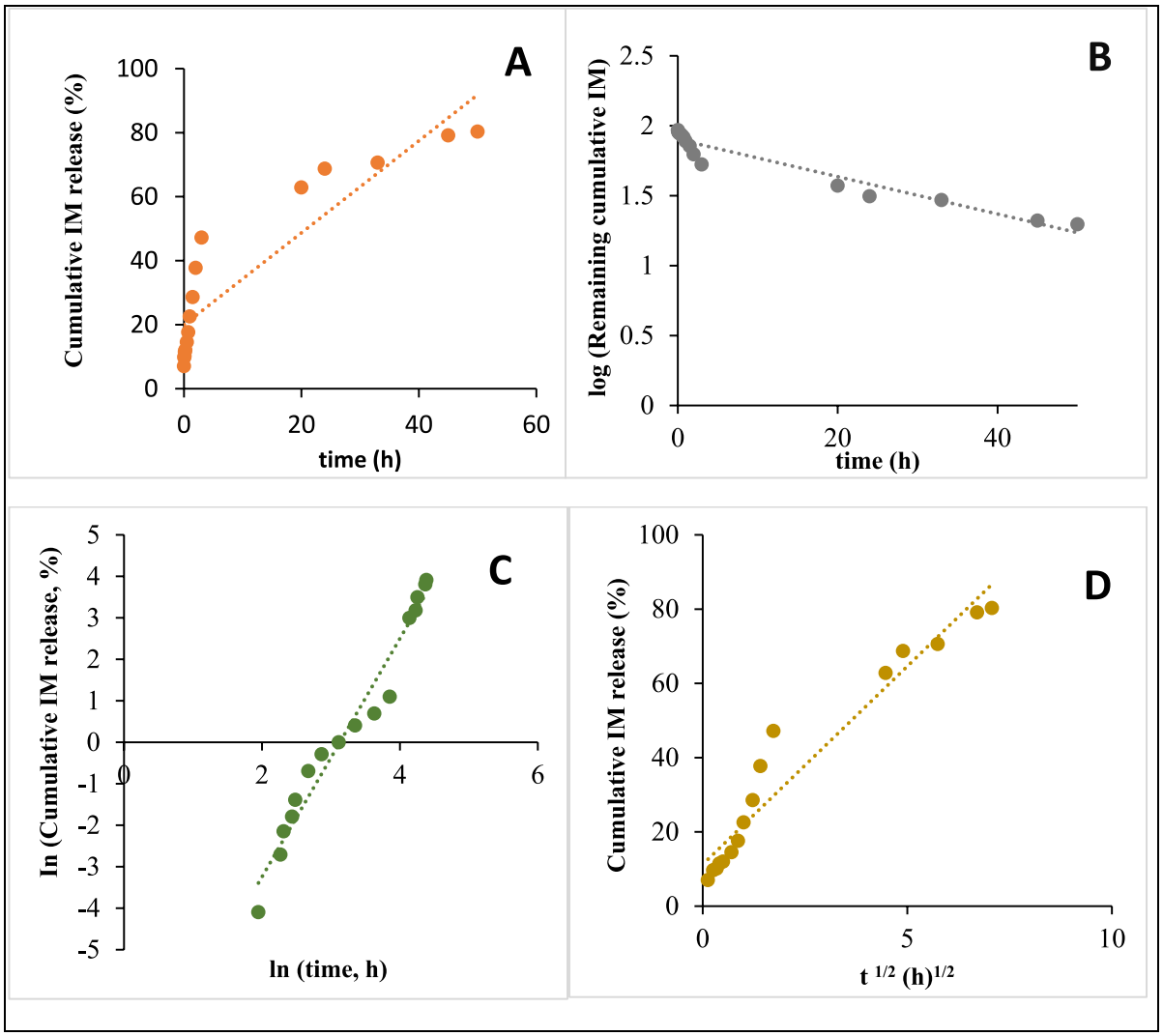


Fig. 7 IM release curves of rGO@ms at pH 5.0: **A** zero order, **B** first order, **C** Korsmeyer–Peppas, **D** Higuchi

weakening of interactions between IM and the rGO@ms surface. The IM release mechanism of rGO@ms was studied using zero-order, first-order, Higuchi, and Korsmeyer–Peppas kinetic models. Computed parameters showed that the Korsmeyer–Peppas model accurately provided the best fit, and the diffusion exponent (n) value exceeded 0.89, indicating an anomalous transport mechanism consistent with super case II behavior, in which multiple release processes contribute simultaneously. Considering the acidic conditions of tumor tissues, the pH-responsive release behavior of rGO@ms offers possible use for site-specific drug delivery in oncological applications.

Acknowledgements This work was funded by Yildiz Technical University Scientific Research Projects Coordination Unit. Project Number: FYL-2023-5637. The authors also would like to thank Assoc. Prof. Esen Bellur Atici R&D Group Manager at DEVA Holding A.S. for providing the Imatinib Mesylate.

Author contributions Tugba Okur: Experiments, Writing – original draft. Deniz Gul: Experiments, Formal analysis, Writing – original draft. Muge Sari Yilmaz: Supervision, Project administration, Experiments, Conceptualization, Formal analysis, Writing – original draft, Writing—review & editing.

Funding Open access funding provided by the Scientific and Technological Research Council of Türkiye (TÜBİTAK).

Data availability The data generated and/or analyzed during the current study are available from the corresponding author upon reasonable request.

Declarations

Competing interests The authors declare no competing interests.

Open Access This article is licensed under a Creative Commons Attribution 4.0 International License, which permits use, sharing, adaptation, distribution and reproduction in any medium or format, as long as you give appropriate credit to the original author(s) and the source, provide a link to the Creative Commons licence, and indicate if changes were made. The images or other third party material in this article are included in the article's Creative Commons licence, unless indicated otherwise in a credit line to the material. If material is not included in the article's Creative Commons licence and your intended use is not permitted by statutory regulation or exceeds the permitted use, you will need to obtain permission directly from the copyright holder. To view a copy of this licence, visit http://creativecommons.org/licenses/by/4.0/.

References

1. Nel J, Elkhoury K, Velot É, Bianchi A, Acherar S, Francius G et al (2023) Functionalized liposomes for targeted breast cancer drug delivery. Bioact Mater 24:401–437. https://doi.org/10.1016/j.bioactmat.2022.12.027
2. Shi H, Huang R, Wu L, Suo W, Wang Y, Pan Y et al (2024) Construction of a MoS2@mSiO2 nanocarrier as a near-infrared/pH dual-responsive platform to control the drug release for anti-tumor. Surfaces and Interfaces 52:104811. https://doi.org/10.1016/j.surfin.2024.104811
3. Fuentes-Garcia JA, Alavarse AC, de Castro CE, Giacomelli FC, Ibarra MR, Bonvent JJ, Goya GF (2021) Sonochemical route for mesoporous silica-coated magnetic nanoparticles towards pH-triggered drug delivery system. Journal of Materials Research and Technology 15:52–67. https://doi.org/10.1016/j.jmrt.2021.08.014
4. Li Z, Huang J, Wu J (2021) pH-sensitive nanogels for drug delivery in cancer therapy. Biomater Sci 9(3):574–589. https://doi.org/10.1039/D0BM01729A
5. Güncüm E, Geyik G, Işıklan N (2024) Magnetic graphene oxide functionalized alginate-g-poly(2-hydroxypropylmethacrylamide) nanoplatform for near-infrared light/pH/magnetic field-sensitive drug release and chemo/phototherapy. Int J Pharm 659:124287. https://doi.org/10.1016/j.ijpharm.2024.124287
6. Wang J, Liu C, Shuai Y, Cui X, Nie L (2014) Controlled release of anticancer drug using graphene oxide as a drug-binding effector in konjac glucomannan/sodium alginate hydrogels. Colloids Surf B Biointerfaces 113:223–229. https://doi.org/10.1016/j.colsurfb.2013.09.009
7. Gao M, Han Z, Wang Z, Zou X, Peng L, Zhao Y, Sun L (2022) Fabrication of a smart drug delivery system based on hollow Ag2S@mSiO2 nanoparticles for fluorescence-guided synergistic photothermal chemotherapy. Microchim Acta 189(10):376. https://doi.org/10.1007/s00604-022-05468-2
8. Parvaneh S, Pourmadadi M, Abdouss M, Pourmousavi SA, Yazdian F, Rahdar A, Díez-Pascual AM (2023) Carboxymethyl cellulose/starch/reduced graphene oxide composite as a pH-sensitive nanocarrier for curcumin drug delivery. Int J Biol Macromol 241:124566. https://doi.org/10.1016/j.ijbiomac.2023.124566
9. Itoo AM, Vemula SL, Gupta MT, Giram MV, Kumar SA, Ghosh B, Biswas S (2022) Multifunctional graphene oxide nanoparticles for drug delivery in cancer. J Control Release 350:26–59. https://doi.org/10.1016/j.jconrel.2022.08.011
10. Das S, Mazumdar H, Khondakar KR, Kaushik A (2025) Machine learning integrated graphene oxide-based diagnostics, drug delivery, analytical approaches to empower cancer diagnosis. BMEMat 3(1):e12117. https://doi.org/10.1002/bmm2.12117
11. Kemeç Aslan S, Hürkan K (2024) A recent update of graphene-based nanomaterials for biomedical applications: focusing on drug delivery and tissue engineering. Carbon-based nanomaterials: synthesis, agricultural, biomedical, and environmental interventions. Springer Nature Singapore, Singapore, pp 219–229. https://doi.org/10.1007/978-981-97-0240-4_11
12. Rai S, Bhujel R, Biswas J, Swain BP (2021) Biocompatible synthesis of rGO from ginger extract as a green reducing agent and its supercapacitor application. Bull Mater Sci 44(1):40. https://doi.org/10.1007/s12034-020-02318-w
13. Punniyakotti P, Aruliah R, Angaiah S (2021) Facile synthesis of reduced graphene oxide using Acalypha indica and Raphanus sativus extracts and their in vitro cytotoxicity activity against human breast (MCF-7) and lung (A549) cancer cell lines. 3 Biotech 11(4):157. https://doi.org/10.1007/s13205-021-02689-9
14. Bairy B, Maity S, Bhowmick S, Ghorai A, Baskey M (2024) Biogenic synthesis of reduced graphene oxide and investigation of adsorption isotherm, kinetics, thermodynamics parameters for water pollution remediation. Graphene 2D Mater 9(1):137–152. https://doi.org/10.1007/s41127-024-00078-6
15. Ghosh S, Das P, Sen MB (2021) Plant extract assisted synthesis of reduced graphene oxide sheet and the photocatalytic performances on cationic and anionic dyes to decontaminate wastewater. Adv Nat Sci Nanosci Nanotechnol 12(1):015008. https://doi.org/10.1088/2043-6254/abde41

16. Dias MI, Barros L, Dueñas M, Alves RC, Oliveira MBPP, Santos-Buelga C, Ferreira ICFR (2014) Nutritional and antioxidant contributions of Laurus nobilis L. leaves: would be more suitable a wild or a cultivated sample? Food Chem 156:339–346. https://doi.org/10.1016/j.foodchem.2014.01.122
17. Dobroslavić E, Repajić M, Dragović-Uzelac V, Elez Garofulić I (2022) Isolation of Laurus nobilis leaf polyphenols: a review on current techniques and future perspectives. Foods 11:235. https://doi.org/10.3390/foods11020235
18. Guo D, Yang H, Zhang Y, Chen L (2019) Constructing mesoporous silica-grown reduced graphene oxide nanoparticles for photothermal-chemotherapy. Microporous Mesoporous Mater 288:109608. https://doi.org/10.1016/j.micromeso.2019.109608
19. Aramideh A, Ashjari M, Niazi Z (2023) Effects of natural polymers for enhanced silica-based mesoporous drug carrier. J Drug Deliv Sci Technol 81:104189. https://doi.org/10.1016/j.jddst.2023.104189
20. Khoz R, Yazdian F, Pourmadadi M, Rahdar A, Fathikarkan S, Pandey S (2024) Current trends in silica based drug delivery systems. Eur J Med Chem Rep 12:100206. https://doi.org/10.1016/j.ejmcr.2024.100206
21. Li S, Cao C, Gao J, Li K, Kang J, Wu D, Kong Y (2021) Dual stimuli-responsive nanoplatform based on core-shell structured graphene oxide/mesoporous silica@alginate. Int J Biol Macromol 175:209–216. https://doi.org/10.1016/j.ijbiomac.2021.02.021
22. Liu X, Wu X, Xing Y, Zhang Y, Zhang X, Pu Q, Wu M, Zhao JX (2020) Reduced graphene oxide/mesoporous silica nanocarriers for pH-triggered drug release and photothermal therapy. ACS Appl Bio Mater 3(5):2577–2587. https://doi.org/10.1021/acsabm.9b01108
23. Khanmohammadi A, Rashidi V, Sadighian S (2023) Reduced graphene oxide/silica nanocomposite as anticancer drug delivery nanocarrier. Biointerf Res Appl Chem 13(4):383. https://doi.org/10.33263/BRIAC134.383
24. Deshmukh PK, Lakade SH, Jaiswal UR, Harde MT, More MP (2022) One step synthesis approach of mesoporous silica packed with graphene oxide nanosheet: characterisation and drug release aspects. Mater Technol 37(11):1677–1690.https://doi.org/10.1080/10667857.2021.1972689
25. Pooresmaeil M, Asl EA, Namazi H (2021) Simple fabrication of biocompatible chitosan/graphene oxide microspheres for pH-controlled amoxicillin delivery. Eur Polym J 159:110706. https://doi.org/10.1016/j.eurpolymj.2021.110706
26. Li R, Wang Y, Du J, Wang X, Duan A, Gao R, Li B (2021) Graphene oxide loaded with tumor-targeted peptide and anti-cancer drugs for cancer target therapy. Sci Rep 11(1):1725. https://doi.org/10.1038/s41598-021-81218-3
27. Gou K, Xin W, Lv J, Ma Z, Yang J, Zhao L, Li H (2023) A pH-responsive chiral mesoporous silica nanoparticles for delivery of doxorubicin in tumor-targeted therapy. Colloids Surf B Biointerfaces 221:113027. https://doi.org/10.1016/j.colsurfb.2022.113027
28. Mo R, Gu Z (2016) Tumor microenvironment and intracellular signal-activated nanomaterials for anticancer drug delivery. Mater Today 19(5):274–283. https://doi.org/10.1016/j.mattod.2015.11.025
29. Yang W, Song FX, Wang S, Zhang L, Zeng X, Li Y (2021) Multifunctional mesoporous silica nanoparticles with different morphological characteristics for in vitro cancer treatment. Colloids Surf A Physicochem Eng Asp 610:125717. https://doi.org/10.1016/j.colsurfa.2020.125717
30. Liu D, Chen C, Hu Y, Wu J, Zheng D, Xie Z, Wang G, Qu D, Li J, Qua D (2018) Reduced graphene-oxide/highly ordered mesoporous SiOx hybrid material as an anode material for lithium ion batteries. Electrochim Acta 273:26–33. https://doi.org/10.1016/j.electacta.2018.04.030
31. Alrahlah A, Khan R, Al-Odayni AB, Leonel Bautista S, Vohra F (2020) Evaluation of synergic potential of rGO/SiO2 as hybrid filler for BisGMA/TEGDMA dental composites. Polymers 12(12):3025. https://doi.org/10.3390/polym12123025
32. Chen L, Zhong X, Yi X, Huang et al (2015) Radionuclide 131I labeled reduced graphene oxide for nuclear imaging guided combined radio and photothermal therapy of cancer. Biomaterials 66:21–28. https://doi.org/10.1016/j.biomaterials.2015.06.043
33. Dahiya M, Awasthi R, Gupta G et al (2022) Optimization studies on imatinib mesylate loaded nanoliposomes using Box-Behnken design. Nano Biomed Eng 14(1):23–37. https://doi.org/10.5101/nbe.v14i1.p23-37
34. Hasandoost L, Akbarzadeh A, Attar H, Heydarinasab A (2017) In vitro effect of imatinib mesylate loaded on polybutylcyanoacrylate nanoparticles on leukemia cell line K562. Artif Cells Nanomed Biotechnol 45(3):665–669. https://doi.org/10.1080/21691401.2016.1175444
35. Depan D, Shah J, Misra RDK (2011) Controlled release of drug from folate-decorated and graphene mediated drug delivery system: synthesis, loading efficiency, and drug release response. Mater Sci Eng C Mater Biol 31(7):1305–1312. https://doi.org/10.1016/j.msec.2011.04.010
36. Ayazi H, Akhavan O, Raoufi M, Varshochian R, Motlagh NSH, Atyabi F (2020) Graphene aerogel nanoparticles for in-situ loading/pH sensitive releasing anticancer drugs. Colloids Surf B Biointerfaces 186:110712. https://doi.org/10.1016/j.colsurfb.2019.110712
37. Narayan R, Gadag S, Garg S, Nayak UY (2022) Understanding the effect of functionalization on loading capacity and release of drug from mesoporous silica nanoparticles: a computationally driven study. ACS Omega 7(10):8229–8245. https://doi.org/10.1021/acsomega.1c06723
38. Wang Y, Wang K, Zhao J, Liu X, Bu J, Yan X, Huang R (2013) Multifunctional mesoporous silica-coated graphene nanosheet used for chemo-photothermal synergistic targeted therapy of glioma. J Am Chem Soc 135(12):4799–4804. https://doi.org/10.1021/ja312004f
39. Costa P, Lobo JMS (2001) Modeling and comparison of dissolution profiles. Eur J Pharm Sci 13(2):123–133. https://doi.org/10.1016/S0928-0987(01)00095-1

Publisher's Note Springer Nature remains neutral with regard to jurisdictional claims in published maps and institutional affiliations.